Wind Engineering Joint Usage/Research Center
FY2020 Research Result Report

Research Field: Wind Hazard Mitigation・Wind-Resistant Construction field
Research Year: FY2020
Research Number: 20202004
Research Theme: Effects of aspect ratio on across-wind response of circular- and square-section super-tall buildings
Representative Researcher: Qingshan, Yang

Budget [FY2020]: 600,000Yen

*There is no limitation of the number of pages of this report.
*Figures can be included to the report and they can also be colored.
*Submitted reports will be uploaded to the JURC Homepage.

1. Research Aim

With great improvement of current society, flexible structures with large aspect ratio such as super-tall buildings, etc., featured with low natural frequency have been constructed in many cities around the world (Fig.1). With decrease of natural frequency, the concerning reduced design wind speed increases, which can approach and even become higher than the critical vortex lock-in wind speed in across-wind direction. Thus, it might trigger the building fatigue or collapse more easily. Both wind tunnel test and full-scale measurement previously indicted that these tall and slender structures are generally governed by their across-wind responses rather than their along-wind responses. Therefore, the across-wind responses of the structures with large aspect ratio must be addressed.

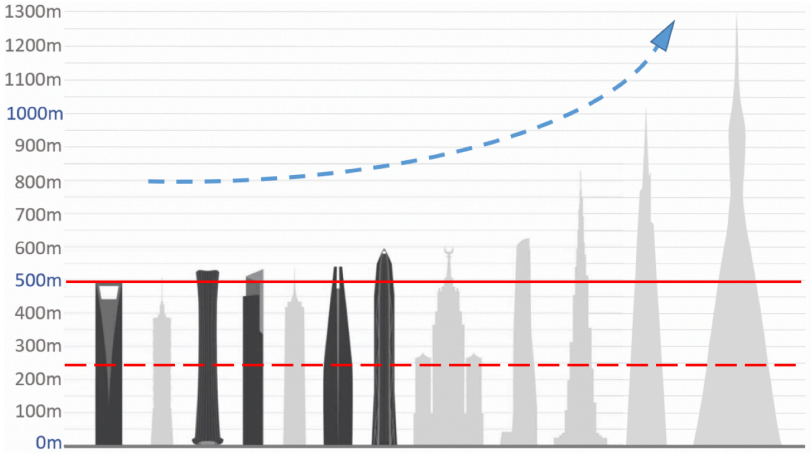

Fig. 1 Constructed and under constructed super tall buildings in the world

The across-wind force acting on the super-tall buildings is composed by stochastic buffeting force and motion-induced force. In order to estimate the crosswind response based on the linear random vibration theory, the stochastic buffeting force can be described in frequency domain by a spectrum. That spectrum usually can be achieved from High Frequency Force Balance (HFFB) or High Frequency Pressure Test (HFPT) in wind tunnel. For the motion-induced force, one component of that is in phase with displacement, which can further be superposed on the structural stiffness, is defined as aerodynamic stiffness; the other component of motion-induced force is in phase with velocity, which can further be superposed on the structural damping, is defined as the aerodynamic damping. The aerodynamic stiffness can usually be ignored because it is rather smaller than structural stiffness. While

the magnitude of aerodynamic damping is quite comparable with structural damping. Moreover, aerodynamic damping becomes negative around the vortex-resonance critical wind speed, and it acts as a source of energy input to the structure. Current research show that, aerodynamic damping is a non-linear function of velocity and/or displacement of vibration, which plays an important role in the generation of crosswind response and determination of response characteristics.

To accurately identify the nonlinear aerodynamic damping of super-tall buildings, methods such as Random decrement technique (RDT), Karman filter (KF), Equivalent nonlinear equations (ENLE) and so forth have been applied in the past. It should be carefully validated that which one is efficient for identifying the nonlinear aerodynamic damping. In fact, the expression of the amplitude dependency of dynamic characters of the full-scale tall buildings is unknown, thus it is necessary to perform the numerical simulations with known expressions of dynamic parameters to validate the above methods first. Then, wind tunnel test on aeroelastic rocking models of squared high-rise buildings will be performed, and nonlinear aerodynamic damping will be identified with the accurate methods. At last, the aero-elastic damping model will be proposed for the sake of building design. Current study aims to validate the application of RDT on identifying the linear and nonlinear damping of a SDOF system by random vibration theory.

Nowadays, RDT has been widely adopted in previous study in order to identify the aerodynamic damping. However, RDT is originally proposed for identifying the structural damping based on the full-scale measurements (e.g., Jeary, 1992 and 1996; Tamura and Suganuma, 1996). Although the identification of the structural damping of full-scale tall and slender structures has shown effective results, it remains unclear whether it is appropriate for identifying the nonlinear aerodynamic damping of the structural across-wind vibration at vicinity of vortex lock-in wind speed. Thus, this study focuses on identifying linear and nonlinear damping by RDT by numerical simulation.

2. Research Method

This section firstly introduces how to simulate the response of a SDOF system with linear damping and nonlinear damping, respectively, then it provides the bases of RDT for further extracting the damping in section 3.

2.1 Simulated response of SDOF system

The vibration equation of system with single degree of freedom is:

$$\ddot{y}(t) + 2\xi\omega\dot{y}(t) + \omega^2 y(t) = f(t) \quad (1)$$

Where, ξ is damping ratio, ω is natural frequency, $f(t)$ is excitation, in this research it is a function of the lift force coefficient C_L of a circular cylinder. The generalized Power Spectrum Density (PSD) of the C_L can be expressed by Vickery & Basu (1983) and shown in Fig. 2:

$$\frac{fS_{CL}(f,z)}{\sigma_{CL}^2(z)} = \frac{f/f_0(z)}{\sqrt{\pi}B(z)} \exp\left\{-\frac{[1-f/f_0(z)]^2}{B^2(z)}\right\} \quad (2)$$

where σ_{CL} is standard deviation (STD) of buffeting lift force coefficient C_L, S_{CL} is power spectral density of buffeting lift force coefficient, $f_0(z)$ is vortex shedding frequency, B is a bandwidth parameter and $B = 0.25$. Thus, the input across-wind buffeting force is narrowband, it can be presented by spectral represent method. Both constant and nonlinear damping ratio are considered separately of the SDOF system. And the equation of motion can be solved by 4th order Runge-Kutta method.

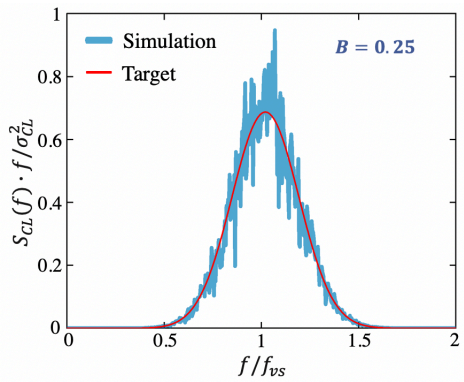

Fig. 2 Form of spectrum of lift force due to vortex shedding.

2.1.1 Response from SDOF system with constant damping

In Eq. (1), considering the natural frequency is equal to 8.1Hz and the constant damping ratio $\xi = \xi_s = 0.75\%$, in which ξ_s means the structural damping. The time history of crosswind response with the 200Hz sampling frequency is shown in Fig. 3. The PDF, PSD and auto-correlation function of crosswind response are shown in Fig. 4. When the SDOF system with a linear damping and a narrowband excitation, the output crosswind response is stationary, narrowband and Gaussian process, it's auto-correlation function is a free vibration decay function.

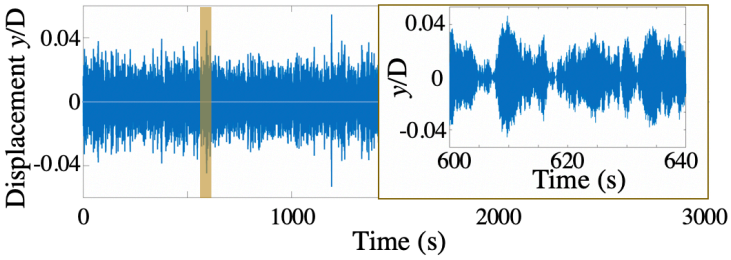

Fig. 3 Time history of crosswind displacement of SDOF system with constant damping

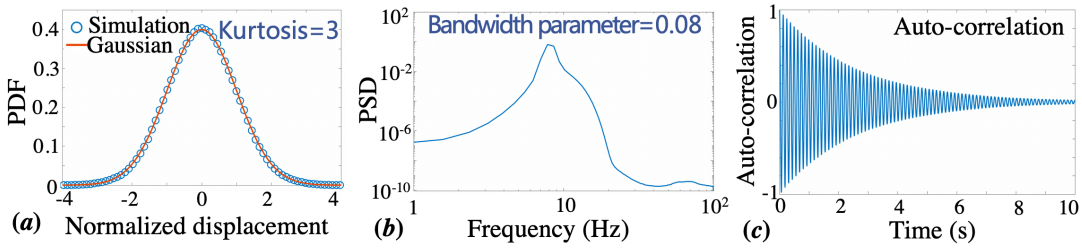

Fig. 4 Properties of crosswind response of SDOF system with constant damping.
(a) PDF; (b) PSD; (c) Auto-correlation function

2.1.2 Response from SDOF system with nonlinear aerodynamic damping

In Eq. (1), considering the natural frequency is equal to 8.1Hz; the damping ratio $\xi = \xi_s + \xi_a$, where ξ_s is structural damping which is equal to 0.75%, and ξ_a is nonlinear aerodynamic damping, in this research it is expressed by Vickery & Basu, 1983; Lupi et.al., 2018 and Guo et.al., 2021 and shown as:

$$\xi_a(U_r) = -\frac{\rho D^2}{m_{eq}} K_a(U_r) \tag{3}$$

In which, the aerodynamic damping parameter $K_a(U_r)$ can be expressed by:

$$K_a(U_r) = K_{a0}(U_r)\left[1 - \varepsilon(U_r)\frac{\Gamma\left(\frac{\beta(U_r)+1}{2}\right)}{\Gamma\left(2+\frac{\beta(U_r)}{2}\right)\Gamma\left(\frac{1}{2}\right)} y_{max}^{\beta(U_r)}\right] \tag{4}$$

Where, $U_r = U/(f_s \cdot D) = (U/U_{cr})/S_t$ is the reduced wind speed, $U_{cr} = (f_s \cdot D)/S_t$ is the vortex-resonance critical wind speed, S_t is the Strouhal number, $K_{a0}(U_r)$ is a factor representing energy input to the structure and varies with U_r, and $\varepsilon(U_r)$ is a parameter that represents the nonlinear dissipation of energy of aerodynamic damping to make the VIV response self-limited. $\beta(U_r)$ represents varying aero-elastic dissipation under different wind speeds and is used for adjusting the curvature of K_a-curves at different wind speeds U/U_{cr} when modeling K_a.

In this case, $K_{a0}(U_r) = 2.648$; $\beta(U_r) = 0.511$ and $\varepsilon(U_r) = 2.47$. Thus, the time history of crosswind response with the 200Hz sampling frequency is shown in Fig. 5. The PDF, PSD and auto-correlation function of crosswind response are shown in Fig. 6. When the SDOF system with the above nonlinear damping and a narrowband excitation, the output crosswind response is stationary, narrowband and Non-Gaussian process, it's auto-correlation function decays slowly and remains relatively large amplitude even after long time.

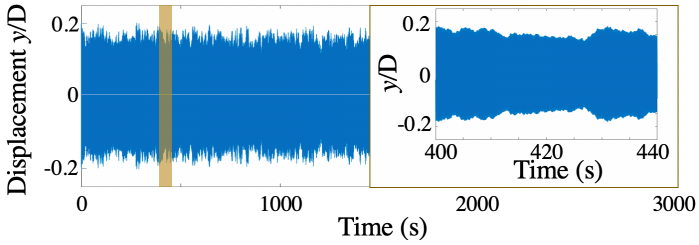

Fig. 5 Time history of crosswind displacement of SDOF system with nonlinear damping

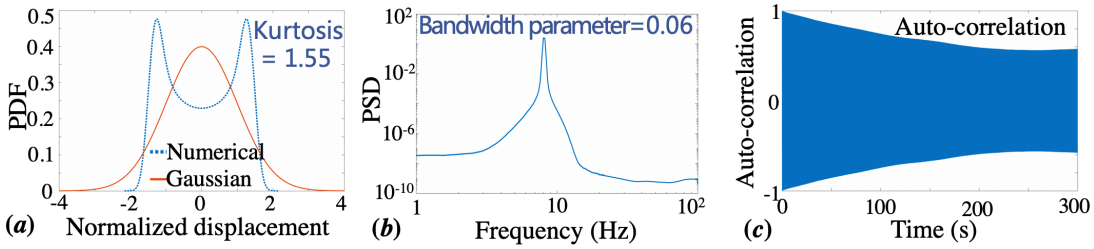

Fig. 6 Properties of crosswind response of SDOF system with nonlinear damping.
(a) PDF; (b) PSD; (c) Auto-correlation function

2.2 Random Decrement Technique

The concept of random decrement technique was initially proposed by Cole (1973) in aerospace industry, which had no strict theoretical basis at that time. The mathematics certification of RDT has been first given by Vandiver et al. (1982). RDT has two characters which can combine dynamic characters with the response amplitudes. Firstly, RDT is a time-domain method in the methods for linear structures and it can capture the time-variant nature of dynamic characters. Secondly, RDT divides the response data into many segments and averages them.

The response of the SDOF system in Eq. (1) can be expressed by:

$$y(t) = y(0)\alpha(t) + \dot{y}(0)v(t) + \int_0^t f(\tau)h(t-\tau)d\tau \qquad (5)$$

Where, $y(0)$ is the initial displacement, $\alpha(t)$ is the free-vibration response with $\alpha(0) = 1$ and $\dot{\alpha}(0) = 0$, $v(t)$ is the free-vibration response with $v(0) = 0$ and $\dot{v}(0) = 1$, and $h(t)$ is the impulse response function.

When $f(t)$ is a zero-mean stationary stochastic process, then with a proper threshold, several segments can be extracted from the response and averaged to get a Random Decrement Signature (RDS) $D(\tau)$:

$$D(\tau) = \frac{1}{M}\sum_{i=1}^{M} y(t_i + \tau) \qquad (6)$$

Where, M is the number of segments. It should be noted that $y(t) \approx y(0)\alpha(t)$ in Eq. (5) when M is sufficiently large. Thus, RDS $D(\tau)$ becomes a free-vibration response with initial displacement $y(0)$ and initial velocity 0. Natural frequency and damping ratio can be estimated from $D(\tau)$.

Jeary (1992 and 1996) has proposed that RDT could be used to identify the amplitude dependency of nonlinear characters using multi-triggering levels, which is identified as Traditional RDT in this research. The method is described as follows:

- Select a set of thresholds a_j, j=1, 2, ..., M.
- For each a_j, calculate the Random Decrement Signal (RDS) $D_j(\tau)$ and estimate the natural frequency and damping ratio by fitting the $D_j(\tau)$ in the form of free-vibration decay curve.
- Arrange the frequencies and damping ratios by thresholds.

Although traditional RDT is convenient and practical, Jeary did not provide a theoretical basis. The identified results using traditional RDT might be questionable.

Tamura and Suganuma (1996) has proposed RDT ranked by peak amplitude, where the theoretical principle has been explained and numerical simulation has been validated, which is identified as Peak RDT in this research. The rationale is that only the peaks are selected as triggering points and other procedures are same as those of traditional RDT. Peak RDT did have the theoretical foundation; however, because of the selection of peak amplitudes whose number of occurrences are much smaller than those of the response data, when the size of the data is not large enough, the resulting average is not ideal.
Huang and Gu (2016) has shorten the response segments into two period according to "Assuming dynamic parameter in a response segment with two periods changes slightly and can be viewed as constants", which is identified as Envelop RDT in this research. The analytical steps are:
- For a response $y(t)$, calculate its envelope $A(t)$ by using the Hilbert transform and treat it as the amplitude envelope.
- Select a set of thresholds a_j, j=1, 2, ..., M.
- For each a_j, cut the amplitude envelope $A(t)$. Points $A_j(t_i)$ on $A(t)$ equaling a_j, and corresponding points $y_j(t_i)$ on response $y(t)$ at instants t_i, i = 1, 2 ,., N, are obtained.
- The segments $y_j(t_i + \tau)$ for a_j are formed by including two periods of data after each $y_j(t_i)$. When the first point of the segment $y_j(t_i + \tau)$ is less than zero, the segment is multiplied by -1.
- To calculate the RDS $D_j(\tau)$ corresponding to a_j, add all the segments for a_j and the segments for adjacent amplitudes a_{j-1} and a_{j+1} whose initial points are smaller than a_j into the average process.
- Estimate the parameters of amplitude a_j from $D_j(\tau)$ by fitting the $D_j(\tau)$ in the form of free-vibration decay curve and arrange the parameters by thresholds to get the amplitude dependency of dynamic parameters.
The advantage of the envelope RDT investigated by numerical simulation is it can identify the non-linear damping more accurate by using a short time series than the above two.
The applicability of traditional RDT, peak RDT, and envelope RDT in evaluating the amplitude dependency of damping ratio are verified and analyzed using numerical simulations.

3. Research Result

3.1 Identification of constant damping

Based on the response of a SDOF system with a constant damping ratio as shown in sub-section 2.1.1, RDS are gained by traditional RDT, peak RDT and envelop RDT individually. Effects of the amplitude and time duration on RDS are addressed. Finally, the identified damping from each RDS has been shown and compared.

3.1.1 Effects of trigger level

The RDS from traditional RDT with thresholds a_j = 0.02, 0.03 and 0.04, respectively, are shown in Fig. 7, the corresponding numbers of segments in 1000s are 7040, 862 and 44. And RDS from Peak RDT with threshold ranges R =0.02 - 0.03, 0.03 - 0.04 and 0.04 - 0.05, respectively, are shown in Fig. 8, the corresponding numbers of segments are 3138, 391 and 14. Each segment is 10s long. Because of the RDS from envelop RDT are quite short, they haven't been shown here. As the result, the RDS from both traditional RDT and peak RDT are sensitive to trigger level.
The identification of constant damping by both traditional and peak RDTs relies on both the trigger level and the amplitude, as shown in Fig. 9 and Fig 10, respectively.

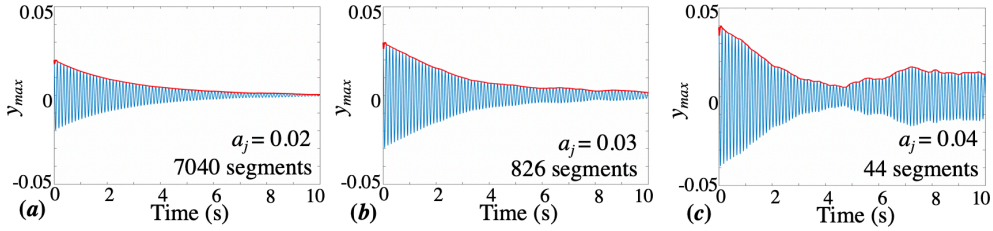

Fig. 7 RDS from traditional RDT with time duration T= 1000s (Constant damping case)

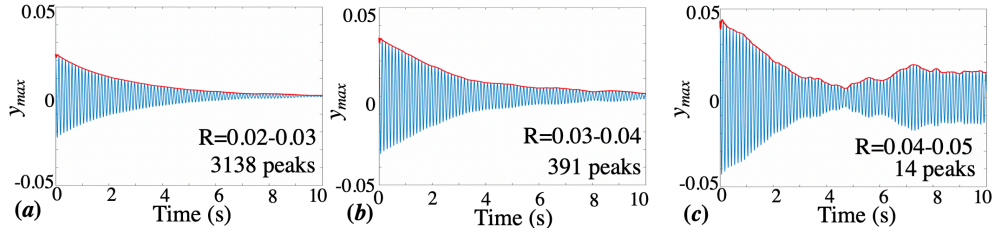

Fig. 8 RDS from Peak RDT with total time duration T= 1000s (Constant damping case)

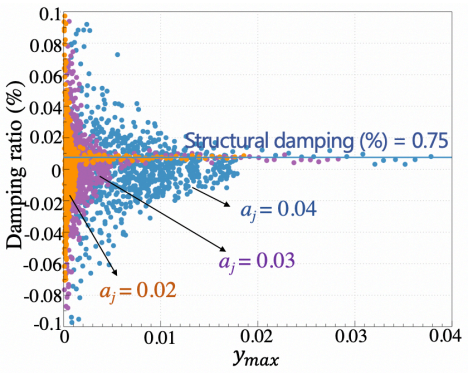

Fig. 9 Identified damping ratio by Traditional RDT with T = 1000s (Constant damping case)

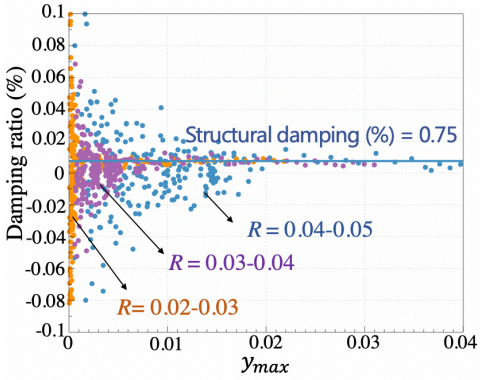

Fig. 10 Identified damping ratio by Peak RDT with T = 1000s (Constant damping case)

3.1.2 Effects of time duration

The RDS from traditional RDT with time durations T=1000s, 500s and 250s, respectively, are shown in Fig. 11, the corresponding numbers of segments are 7040, 988 and 514. And RDS from peak RDT with time durations T=1000s, 500s and 250s, respectively, are shown in Fig. 12, the corresponding numbers of segments are 1002, 559 and 323. As the result, the RDS from both traditional RDT and peak RDT are relatively sensitive to time duration.

The identified constant damping by both traditional and peak RDTs are shown in Fig. 13 and Fig 14, respectively. Though the identified constant damping relies on the time duration, however, that relies on the trigger level more when the time duration isn't so small.

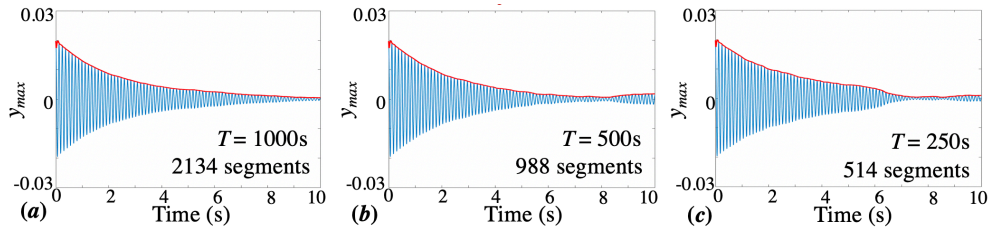

Fig. 11 RDS from Traditional RDT with threshold a_j = 0.03 (Constant damping case)

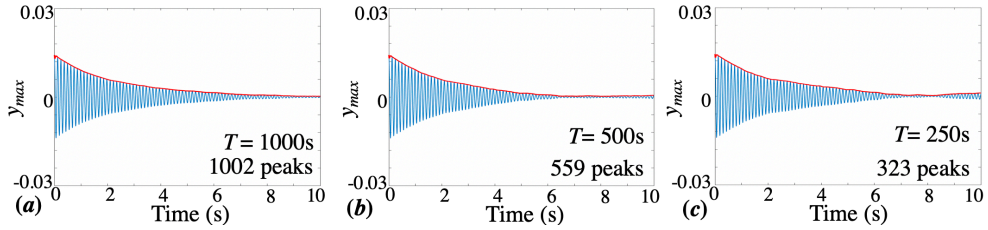

Fig. 12 RDS from Peak RDT with peak range R =0.03 - 0.04 (Constant damping case)

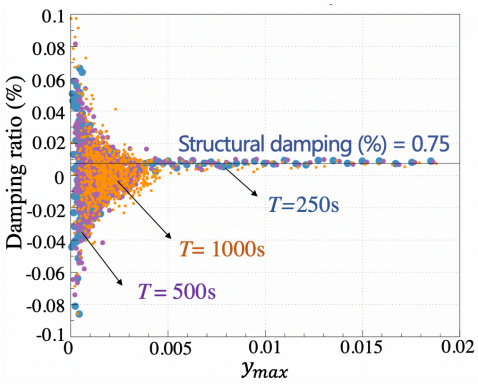

Fig. 13 Identified damping ratio by Traditional RDT with threshold a_j = 0.03 (Constant damping case)

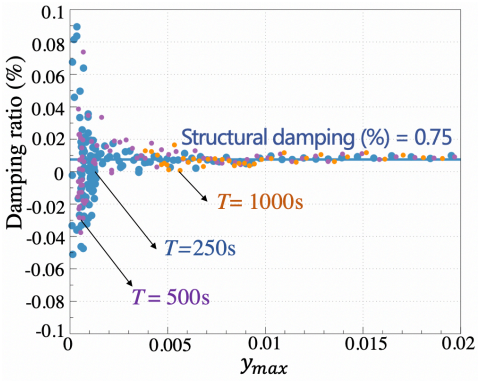

Fig. 14 Identified damping ratio by Peak RDT with range R =0.03 - 0.04 (Constant damping case)

3.1.3 Comparison of three RDTs

Based on the analysis in 3.1.1 and 3.1.2, all trigger levels and sufficient long duration T = 3000s are considered to get the more reasonable RDS. RDS from traditional RDT with threshold a_j = 0.02 is shown in Fig. 15(a); RDS from peak RDT with peak range R =0.02 - 0.03 is shown in Fig. 15(b); and RDS from envelop RDT is with peak range R =0.01 - 0.02, which isn't shown. The identified damping ratios from the above three RDSs are shown in Fig. 15(c). As the result, All the above three RDTs are efficient for identifying the constant damping ratio from a narrowband Gaussian process.

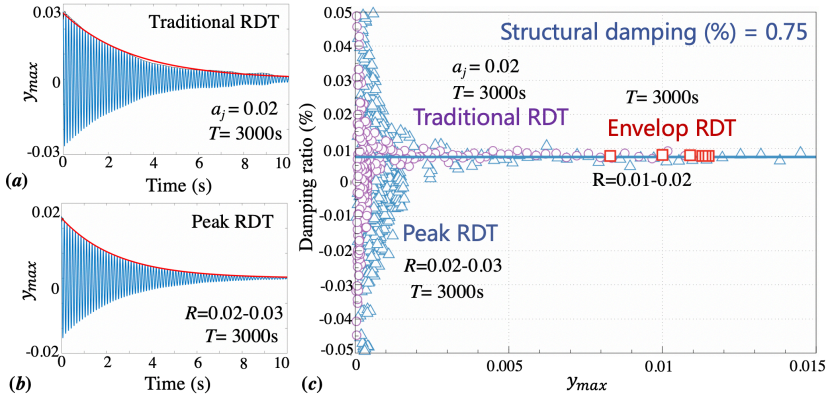

Fig. 15 RDSs and identified damping ratios from traditional RDT, peak RDT and envelop RDT. (Constant damping case)

3.2 Identification of non-linear damping

Based on the response of a SDOF system with a nonlinear aerodynamic damping as shown in section 2.1.2, RDS are gained by traditional RDT, peak RDT and envelop RDT individually. Effects of the amplitude and time duration on RDS are addressed. Finally, the identified damping from each RDS has been shown and compared.

3.2.1 Effects of Thresholds a_j or R

The RDS from traditional RDT with thresholds a_j = 0.05, 0.16 and 0.2, respectively, are shown in Fig. 16, the corresponding numbers of segments in 1000s are 12961, 5343 and 17. And RDS from Peak RDT with threshold ranges R =0.11 - 0.12, 0.15 - 0.16 and 0.19 - 0.2, respectively, are shown in Fig. 17, the corresponding numbers of segments are 30, 1140 and 77. Each segment is 10s long. As the result, the RDS from both traditional RDT and peak RDT are not coincidence with the free decay function, and they rely on the trigger level.

The identified damping by traditional RDT are far away from the target nonlinear damping, as indicated in Fig. 18. While the identified damping by peak RDT are fluctuating around the target nonlinear damping function when the amplitude is around 0.12~0.2, as indicated in Fig. 19.

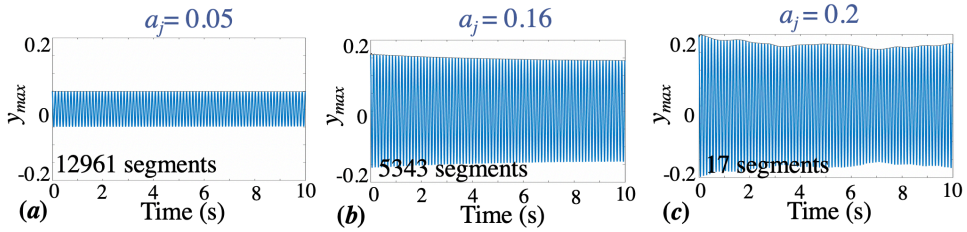

Fig. 16 RDS from traditional RDT with time duration T= 1000s (Nonlinear damping case)

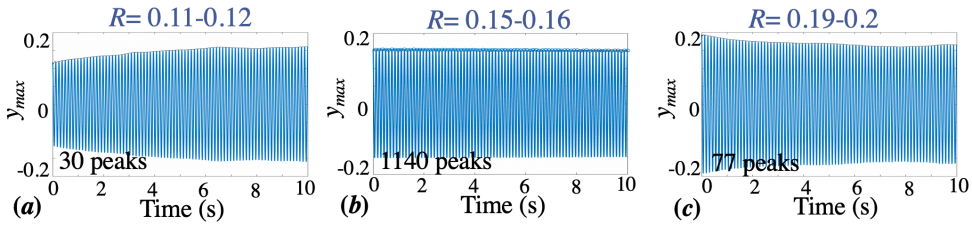

Fig. 17 RDS from peak RDT with time duration T= 1000s (Nonlinear damping case)

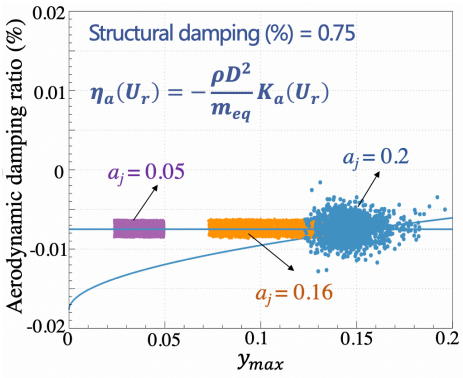

Fig. 18 Identified damping ratio by Traditional RDT with T = 1000s (Nonlinear damping case)

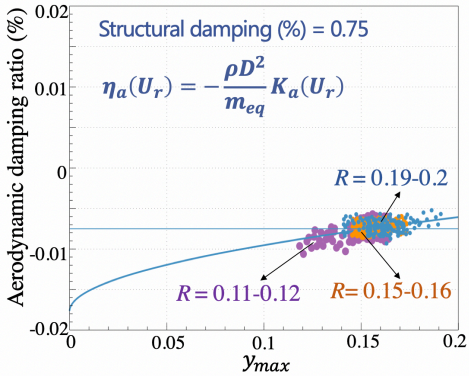

Fig. 19 Identified damping ratio by Peak RDT with T = 1000s (Nonlinear damping case)

3.2.2 Effects of time duration

The RDS from traditional RDT with time durations T=1000s, 500s and 250s, respectively, are shown in Fig. 20, the corresponding numbers of segments in 1000s are 5343, 2773 and 1175. And RDS from Peak RDT with time durations T=1000s, 500s and 250s, respectively, are shown in Fig. 21, the corresponding numbers of segments are 1884, 1000 and 525. Each segment is 10s long. As the result, the RDS from both traditional RDT and peak RDT are not coincidence with the free decay function, and they aren't affected much by the time duration. The identified damping by both traditional RDT and peak RDT are concentrated at the intersection of the structural damping ratio and nonlinear aerodynamic damping ratio, when they at a proper trigger level as indicated in Fig. 22 and Fig. 23.

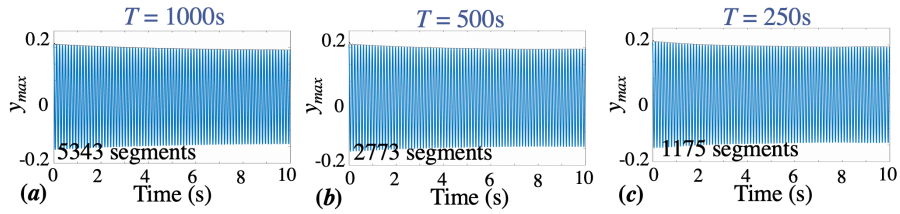

Fig. 20 RDS from traditional RDT with threshold $a_j = 0.16$ (Nonlinear damping case)

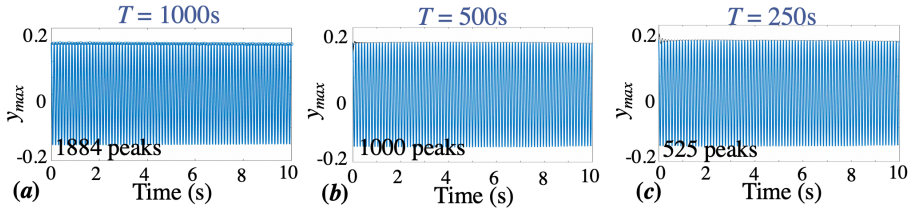

Fig. 21 RDS from traditional RDT with peak range $R = 0.15 - 0.16$ (Nonlinear damping case)

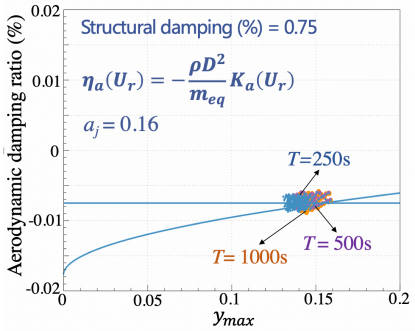

Fig. 22 Identified damping ratio by Traditional RDT with threshold $a_j = 0.16$ (Nonlinear damping case)

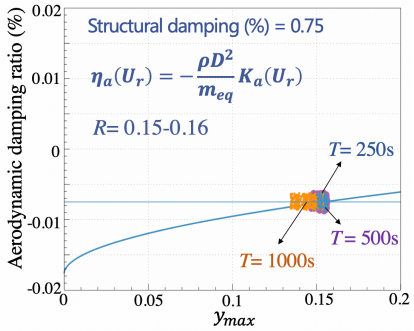

Fig. 23 Identified damping ratio by Traditional RDT with peak range $R = 0.15 - 0.16$ (Nonlinear damping case)

3.2.3 Comparison of three RDTs

Based on the analysis in 3.2.1 and 3.2.2, all trigger levels and sufficient long duration $T = 3000s$ are considered to get the more reasonable RDS. RDS from traditional RDT with threshold $a_j = 0.16$ is shown in Fig. 24(a); RDS from peak RDT with peak range R =0.15 - 0.16 is shown in Fig. 24(b); and RDS from envelop RDT is with peak range R =0.14 - 0.15, which isn't shown. The identified damping ratios from the above three RDSs are shown in Fig. 24(c). As the result, when identifying the nonlinear aerodynamic damping, traditional RDT is failed; peak RDT performs better but isn't accurate enough; as a special case of peak RDT, envelop RDT performs accurately in a certain amplitude range R =0.11 - 0.16.

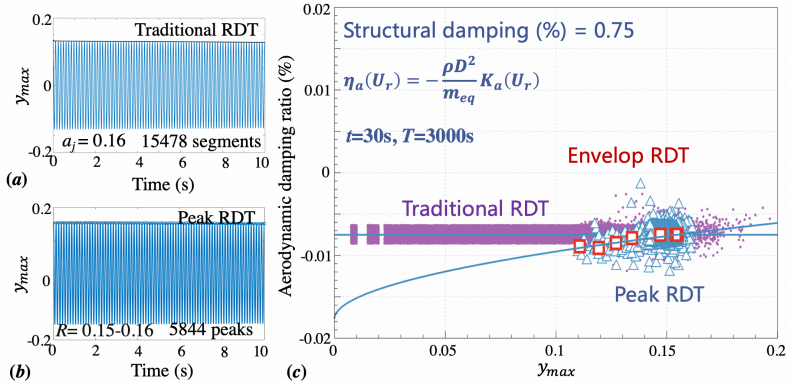

Fig. 24 RDSs and identified damping ratios from traditional RDT, peak RDT and envelop RDT. (Nonlinear damping case)

4. Published Paper etc.

[Underline the representative researcher and collaborate researchers]
[Published papers]
1. None
[Presentations at academic societies]
1. None
[Published books]
1. None
[Other]
Intellectual property rights, Homepage etc.

5. Research Group

1. Representative Researcher
   Qingshan, Yang
2. Collaborate Researchers
   1. Yong Chul, Kim
   2. Yukio, Tamura
   3. Wenshan, Shan
   4. Kunpeng, Guo

6. Abstract (half page)

Research Theme: Effects of aspect ratio on across-wind response of circular- and square-section super-tall buildings

Representative Researcher (Affiliation): Qingshan, Yang (Chongqing University)

Summary・Figures

By numerical simulation of the response of a SDOF system with constant damping and nonlinear damping, respectively, traditional RDT, peak RDT and envelop RDT are validated for identifying the linear and nonlinear damping. The results show that:

1)For identifying the constant damping from a linear system, traditional RDT, peak RDT and envelop RDT performs accurate results.

2) For identifying the nonlinear aerodynamic damping from the nonlinear system, traditional RDT is failed; peak RDT performs better but isn't accurate enough; as a special case of peak RDT, envelop RDT performs accurately in a certain amplitude range.